Available online at www.sciencedirect.com
ScienceDirect
Acta Materialia 58 (2010) 531–540
Acta MATERIALIA
www.elsevier.com/locate/actamat

First-principles study of solute–vacancy binding in magnesium

Dongwon Shin, Christopher Wolverton *

Department of Materials Science and Engineering, Northwestern University, Evanston, IL 60208, USA

Received 22 July 2009; received in revised form 10 September 2009; accepted 13 September 2009
Available online 14 October 2009

Abstract

Solute–vacancy binding is a key quantity in understanding diffusion kinetics, and may also have a considerable impact on the hardening response in Mg alloys. However, the binding energetics between solute impurities and vacancies in Mg are notoriously difficult to measure accurately and are largely unknown. Here, we present a large database of solute–vacancy binding energies in Mg from first-principles calculations based on density functional theory. Our vacancy formation energy and dilute mixing energy, which are byproducts of the solute–vacancy binding calculations, show good agreement with experiments, where available. We have investigated the simple physical effects controlling solute–vacancy binding in Mg and find that there is a modest correlation between binding energy and solute size, with larger solute atoms more favorably binding with neighboring vacancies to relax the strain induced by the solutes. Most early 3*d* transition metal solutes do not favorably bind with vacancies, indicating that a simple bond-counting argument is not sufficient to explain the trends in binding, in contrast to the case of binding in Al. We also predict positive vacancy binding energies for some commonly used microalloying elements in Mg which are known to improve age hardenability, i.e. Na, In, Zn, Ag and Ca. Even larger vacancy binding energies are found for some other solutes (e.g. Cu, Sn, Pb, Bi and Pt), which await experimental validation.

Keywords: Solute–vacancy binding; Magnesium alloys; First-principles calculations

1. Introduction

Lightweight alloys, such as those based on Mg, have attracted significant attention for potential automotive application. However, the use of Mg alloys in certain applications remains limited because of their relatively low strength compared with those of Al alloys and steels. Consequently, a significant research effort is being focused on improving mechanical strength in Mg alloys. Precipitation hardening is one of many strengthening mechanisms that may be used to further improve the strength of Mg alloys. The precipitation-hardening response depends upon the size, distribution and volume fraction of precipitates. Solute diffusion kinetics is a key factor controlling the formation of precipitates in Mg alloys, and solute–vacancy binding plays an important role in a quantitative understanding of diffusion.

Solute–vacancy binding in Mg can also play an important role in understanding microalloying additions. It has been shown experimentally [1–4] that trace or microalloying additions to Mg alloys can modify the dispersion and morphology of precipitates to achieve higher strength by altering the atomic clustering processes, which occur prior to nucleation of precipitates. It has been proposed that the relative binding energy between solutes and vacancies may have a considerable impact on determining which clustering processes are dominant and, in turn, which precipitate nucleation processes occur. However, despite the importance of these binding energetics between solutes and vacancies, these binding energies are notoriously difficult to measure, and are also largely unknown in the case of Mg alloys.

We have recently demonstrated that first-principles density functional calculations provide a quantitatively accurate prediction—in comparison with the most accurate experimental equilibrium measurements—of these binding energies in Al [5]. However, such reliable equilibrium measurements for solute–vacancy binding energy do not exist

* Corresponding author.
E-mail address: c-wolverton@northwestern.edu (C. Wolverton).

1359-6454/$36.00
doi:10.1016/j.actamat.2009.09.031

in Mg for any solutes. Hence, in this paper, we use first-principles calculations to predict these vacancy-binding energies of various solutes in Mg, and call for future experiments to test these predictions. For the present work, we select a large number of solutes, including both common solutes in commercial Mg alloys (e.g. Al and Zn) as well as elements that have exhibited potential as effective microalloying elements (e.g. Na, In, Ag and Ca). In addition, we wish to go beyond these few elements, and construct an extensive first-principles database of predicted solute–vacancy bindings for a wide variety of important alloying elements for commercial Mg alloys: Li, Si, K, Sc, Ti, V, Cr, Mn, Fe, Co, Ni, Cu, Ga, Ge, As, Sr, Y, Zr, Nb, Mo, Cd, Sn, Sb, Pt, Au, Ba, Pb and Bi. We then analyze the trends in the binding energies in terms of simple physical features, such as solute size, phase stability, bond-counting arguments and lattice parameter change induced by the addition of solute atoms in hexagonal close-packed (hcp) Mg.

We find that there is a correlation between vacancy binding energy and solute size, i.e. larger solute atoms tend to bind more favorably with vacancies to relax the strain induced by the solute atoms. Most early 3*d* transition metals exhibit unfavorable binding with vacancies in Mg, which is surprising because they commonly do not bind favorably with Mg. This indicates that a simple bond-counting argument is not sufficient to explain unfavorable binding with vacancies for most early 3*d* metals, in contrast to the case of binding in Al. We also predict positive vacancy binding energies for microalloying elements, which are known to improve age hardenability in Mg alloys, i.e. Na, In, Zn, Ag and Ca. Some other solutes (e.g. Cu, Sn, Pb, Bi and Pt) are found to have even larger vacancy binding energies, which await experimental validation.

2. First-principles methodology

We use the Vienna Ab initio Simulation Package (VASP) [6,7] based on density functional theory (DFT) to perform the electronic structure calculations. We use the projector augmented wave (PAW) method [8] and the generalized gradient approximation (GGA) [9,10] for the exchange-correlation functional. All calculations are fully relaxed with respect to all degrees of freedom, i.e. volume, cell vectors and internal atomic positions.

We have used defect Mg supercells to calculate the solute–vacancy binding energies for various solute–vacancy pair spacings. To minimize interactions due to periodic image, we have used the orthorhombic unit cell with four atoms as a basis to construct different size supercells as illustrated in Fig. 1. We have distinguished two inequivalent nearest-neighbor lattice sites for vacancies, with solute atoms placed at the origin of orthorhombic supercell.

Table 1 summarizes the supercell dimensions and *k*-point meshes used for the orthorhombic supercells in the present work. Extensive energy convergence tests indicate that an energy cutoff of 346 eV gives binding energies converged to within 0.01 eV. For magnetic solute elements, namely Cr, Mn, Fe, Co and Ni, we have performed spin-polarized calculations and have used the interpolation scheme suggested by Vosko et al. [11] for the correlation part of the exchange-correlation functional. In addition to above conventional magnetic elements, we also have considered spin-polarized calculations for V (discussed below).

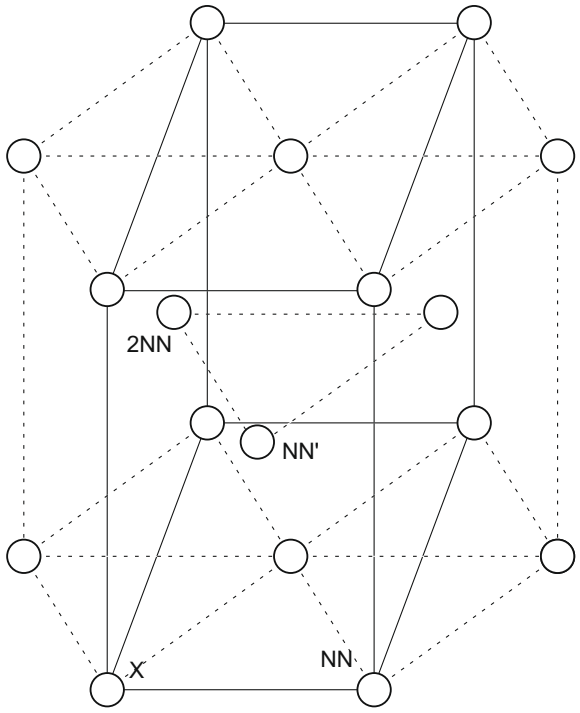

Fig. 1. Schematic diagram of the orthorhombic Mg unit cell (solid lines) used to generate supercells in the present work. The solute atom, X, is at the origin of the supercell and the vacancy is placed at either the nearest-neighbor (NN) or second nearest neighbor (2NN) position. Two inequivalent NN sites are possible in hcp, one at the basal plane and the other one out of the basal plane, and they are distinguished as NN and NN′.

Table 1
Supercell dimensions (based on the orthorhombic cell of Fig. 1) and *k*-point meshes used in the present work. The Monkhorst–Pack scheme [32] was used for the Brillouin zone sampling.

Lattice sites	Supercell size	*k*-Points	Ratio (*a*:*b*:*c*)
48	$3\times2\times2$	$12\times12\times12$	1:1.15:1.09
64	$4\times2\times2$	$10\times10\times10$	1:0.87:0.82
96	$4\times2\times3$	$8\times8\times8$	1:0.87:1.23
144	$4\times3\times3$	$6\times6\times6$	1:1.30:1.23

The solute–vacancy binding energy E_{bind} is defined as follows:

$$-E_{\text{bind}}(\text{X}-\square) = E(\text{Mg}_{N-2}\text{X}_1\square_1) + E(\text{Mg}_N) - E(\text{Mg}_{N-1}\text{X}_1) - E(\text{Mg}_{N-1}\square_1) \quad (1)$$

where $\square$ and X represent a vacancy and a solute atom in the Mg supercell, and N is the number of lattice sites considered. It should be noted in here that the minus sign in Eq. (1) is to keep the solute–vacancy binding energies calculated in this paper consistent with the sign convention

in the literature: a positive binding energy indicates a favorable binding. When we consider a solute–vacancy pair, we put solute atoms at the origin and vacancies at the hcp lattice sites of nearest-neighbor (NN) and second nearest neighbor (2NN) positions, respectively. We also distinguish the two inequivalent NN sites for the vacancy: the one in the same basal plane as the solute (NN) and the other one out of the basal plane of the solute (NN′). Due to the non-ideal (slightly compressed) c/a ratio of hcp Mg[1], the NN pair is slightly longer than the NN′ pair.

As by-products of the solute–vacancy binding calculation, we also obtain the vacancy formation energy in Mg:

$$E_{\mathrm{vac}}(\square) = E(\mathrm{Mg}_{N-1}\square_1) - \frac{N-1}{N}E(\mathrm{Mg}_N) \quad (2)$$

and the dilute mixing energy for X in an hcp Mg solid solution:

$$E_{mix}(\mathrm{X}) = E(\mathrm{Mg}_{N-1}\mathrm{X}) - \frac{N-1}{N}E(\mathrm{Mg}_N) - E(\mathrm{X}) \quad (3)$$

with respect to pure hcp Mg and pure X in its equilibrium structure.

In addition to energetic properties, our first-principles calculations of defect Mg supercells also provide insights into the structure of the defects considered. In order to get a quantitative measure of the atomic size of each solute impurity, X, we also calculate the impurity volume, V^{X}_{imp}, which is given by the volume difference induced by placing a single solute impurity into pure Mg:

$$V^{\mathrm{X}}_{imp} = V(\mathrm{Mg}_{N-1}\mathrm{X}) - V(\mathrm{Mg}_N) \quad (4)$$

In addition to volume changes upon insertion of solutes in Mg, the hcp lattice parameters, a and c, can also relax anisotropically. We also obtain the lattice parameter changes from our first-principles calculations of the $\mathrm{Mg}_{N-1}\mathrm{X}$ supercells. Since this type of anisotropic relaxation is not allowed in cubic elements due to symmetry, the lattice parameter changes in Mg will provide interesting insights into the relaxation of solute impurities in Mg.

3. Results

3.1. Effects of supercell size and defect pair spacing

We begin by investigating the effect of supercell size on the solute–vacancy binding energy in Mg. We have calculated vacancy-binding energies of several different solutes, i.e. Ca, Ti, Zn, Sr, Y and Zr, for the "basal plane" NN solute–vacancy pair. Table 2 gives calculated binding energies of these elements with different size supercells, when $N = 48$, 64, 96 and 144, respectively. We find that 64-atom calculations are generally converged (with the possible exception of Y and Sr). We note that although Sr has a much larger atomic radius (2.15 Å) than that of Mg (1.60 Å), the 64-atom supercell calculation is still well converged. Hence, all results given below for vacancy-binding energies are for 64-atom supercells, unless otherwise specified.

Table 2
Supercell size convergence of NN solute–vacancy binding energies. Binding energies are computed for supercell sizes of 48, 64, 96 and 144 atoms. Solute atoms are placed at the origin of each supercell and vacancies are placed at the lattice site of the NN on the basal plane.

Solute	Solute–vacancy binding energy (eV)			
	48 atoms	64 atoms	96 atoms	144 atoms
Ca	0.05	0.06	0.07	0.09
Ti	−0.23	−0.21	−0.20	−0.21
Zn	0.05	0.05	0.05	0.05
Sr	0.22	0.21	0.23	0.28
Y	−0.11	−0.13	−0.07	−0.07
Zr	−0.28	−0.24	−0.24	−0.24

We also investigate the convergence of the calculated solute–vacancy binding energy for NN and NN′ pairs with respect to supercell size. Table 3 shows the differences in solute–vacancy binding energy between NN and NN′ pairs. In general, the vacancy-binding energy in Mg is not sensitive to the difference between basal plane (NN) and out of basal plane (NN′) nearest-neighbors. All results given below for the solute–vacancy binding are for the NN pair, unless otherwise specified.

3.2. Vacancy formation energy in Mg

We would have liked to validate our first-principles binding energies by comparing them with accurate experimental measurements. Unfortunately, there are not many experimental measurements available for solute–vacancy binding energy in Mg, and none of the measured binding energies are from equilibrium lattice parameter/length measurements. This latter type measurement was shown to be crucial for obtaining quantitatively accurate binding energies in Al [12,5]. However, the vacancy formation energy in Mg is a byproduct of the solute–vacancy binding energy calculation, and there have been many attempts to measure and calculate this quantity. Thus, we validate our first-principles results against experimental measurements for the vacancy formation energy in Mg.

Previously measured [13–17] and calculated [18,19] values for the vacancy formation energy in Mg are summarized in Table 4 along with our current calculations and are in good agreement. Chetty et al. [18] and Krimmel and Fahnle [19] have studied vacancies in Mg from first principles, and both have used the local density approximation (LDA) [20,21]. To compare with these previous calculations, we also calculated vacancy formation with the LDA for different-sized supercells, i.e. 48, 64, 96 and 144, and successfully reproduced the previous result of 0.83 eV. As Table 4 shows, the vacancy formation energies in Mg calculated with the LDA agrees better with experiments than that calculated with the GGA. Carling et al. [22] found the same trend between their first-principles cal-

[1] $c/a = 1.623$ and 1.618 from experiment and DFT, respectively, compared to the ideal value of $\sqrt{\frac{8}{3}} = 1.633$.

Table 3
Comparison of solute–vacancy binding energies for the two different NN pairs in the hcp lattice. Energies are computed for different supercell sizes: 48, 64, 96 and 144 atoms. Solute atoms are placed at the origin of each supercell. Vacancies are placed at a nearest-neighbor site on the basal plane (NN) or at a nearest-neighbor site out of the basal plane (NN′), respectively, as illustrated in Fig. 1.

Lattice	Solute–vacancy binding energy (eV)									
	Ca		Ti		Sr		Y		Zr	
Sites	NN	NN′	NN	NN′	NN	NN′	NN	NN′	NN	NN′
48	−0.05	−0.08	−0.23	−0.20	0.22	0.28	−0.11	−0.07	−0.28	−0.24
64	−0.06	−0.09	−0.21	−0.21	0.21	0.26	−0.13	−0.12	−0.24	−0.25
96	−0.07	−0.09	−0.20	−0.22	0.23	0.27	−0.07	−0.07	−0.24	−0.27
144	−0.09	−0.08	−0.21	−0.23	0.28	0.27	−0.07	−0.07	−0.24	−0.26

Table 4
Comparison of experimental and calculated vacancy formation and solute–vacancy binding energies in Mg. The vacancy formation energy was calculated from supercells with lattice sites $N = 48$, 64, 96 and 144. Solute–vacancy binding energies from first-principles DFT calculations (present work) are from fully relaxed, VASP (64-atom) supercell calculations. All DFT results use the GGA, unless otherwise specified.

	First-principles DFT		Previous works	
	This work[a]	Value	Method	Ref.
Vacancy formation (eV)				
	0.74 ± 0.05	0.89 ± 0.06	Exp ($\Delta\rho_q$)	[13]
	0.83 ± 0.01[b]	0.81 ± 0.02	Exp ($\Delta\rho_{eq}$)	[14]
		0.58 ± 0.01	Exp (DD)	[15]
		0.79 ± 0.03	Exp ($\Delta\rho_q$)	[16]
		0.90 ± 0.1	Exp (PAS)	[17]
		0.83[c]	DFT	[18]
		0.83 ± 0.07[d]	DFT	[19]
Solute–vacancy binding (eV)				
Zn–□	0.05	0.07 ± 0.02	Exp ($\Delta\rho_q$)	[24]
Al–□	0.03	0.29 ± 0.02	Exp (H_v)	[25]

$\Delta\rho_{q,eq}$: electrical resistivity of quenched, thermal equilibrium samples, respectively, H_v, Vickers hardness; DD, differential dilatometry; PAS, position-annihilation spectroscopy.

[a] Variation is given for the calculations with different size supercells.
[b] LDA, $N = 48$, 64, 96 and 144.
[c] LDA, $N = 96$.
[d] LDA, $N = 16$, 36 and 54.

culations (LDA and GGA) and experiments for vacancies in Al. This trend is somewhat surprising since one might typically expect GGA calculations to be more accurate. Carling et al. [22] showed that the resolution of this apparent contradiction is due to an energy correction term necessary because the current approximations for the exchange-correlation potential do not provide an accurate description for the evanescent electron density regions. These authors [22] reported the energy correction term for the vacancy formation in Al for the LDA (0.06 eV) is smaller than that for the GGA (0.15 eV) since the LDA accidentally describes the internal surface created by forming a vacancy better than the GGA. Such correction terms for the vacancy formation energy in Mg have not yet been evaluated for either the LDA or GGA, but our calculations suggest that for Mg (as for Al), the correction for the LDA would be smaller than for the GGA. Nonetheless, the use of such an energy correction term for the vacancy formation is not needed in our first-principles solute–vacancy binding energy calculations since such internal surface effect is cancelled out by the difference between $E(\mathrm{Mg}_{N-2}\mathrm{X}_1\square_1)$ and $E(\mathrm{Mg}_{N-1}\square_1)$ terms as shown in Eq. (1).

3.3. Mg lattice parameters

As another test of the accuracy of our calculations, we consider the effect of alloying additions on the lattice parameters of hcp Mg. Nayeb-Hashemi and Clark [23] compiled experimental measurements of Mg lattice parameter changes induced by various solutes, and we find our calculations are in qualitatively good agreement with experiments, as shown in Fig. 2. Calculated lattice parameters are from fully relaxed 64-atom $\mathrm{Mg}_{63}\mathrm{X}$ supercell calculations. Due to the independent relaxation of a and c lattice parameters, several interesting cases of anisotropic relaxation exist, and our first-principles calculations describe even these cases quite well. For instance, alloying Sc or Pb increases the lattice parameter a in Mg, but only the addition of Pb increases c, while that of Sc does not make any notable difference in c. Our results agree with this observation. It is also shown in Ref. [23] that small additions of In and Sn to Mg increase c of Mg, but not a, and our calculations also give this trend. All other elements that have been discussed in Ref. [23], namely Ag, Al, Cd, Ga, Li, Mn and Zn, are reported to decrease both lattice parameters a and c of hcp Mg, and our calculations also successfully reproduce these experimental observations. This good agreement in structural quantities adds confidence to the accuracy of our first-principles calculations.

3.4. Validating the first-principles binding energies

As stated above, no accurate equilibrium measurements of solute–vacancy binding exist in Mg alloys. Nevertheless we wish to compare our first-principles vacancy-binding energies in Mg with the experimental data which is available. Vydyanath et al. [24] and Rao and Suryanarayana [25] have measured vacancy-binding energies of Zn and Al, respec-

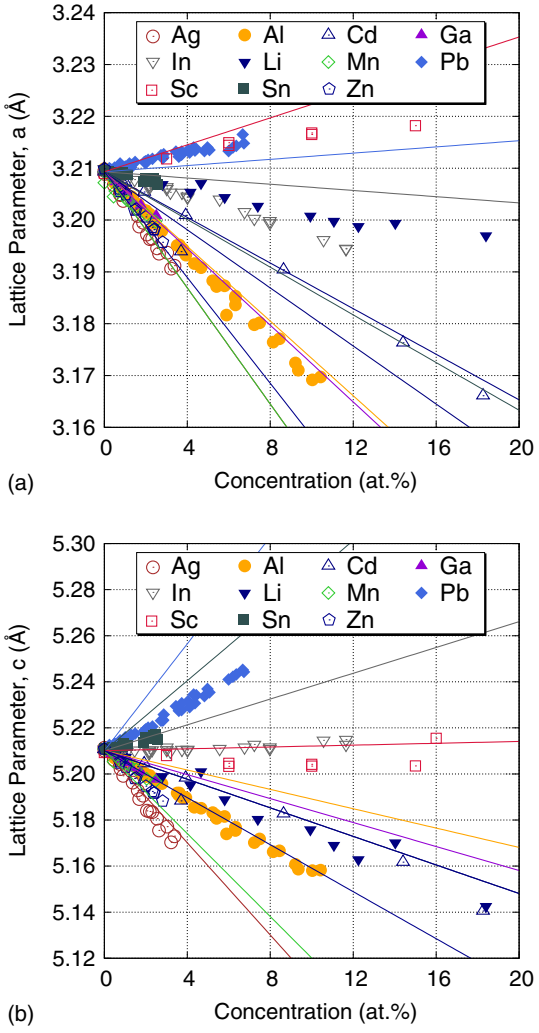

Fig. 2. The effect of alloying additions in the hcp phase on the (a) *a* and (b) *c* lattice parameters of Mg from Ref. [23] (compilation of experimental measurements). Lines represent the lattice parameter changes from first-principles calculations of $Mg_{63}X$ supercells. The same color has been used for both experiments (symbol) and first-principles (line) for each element.

tively, both determined from quenching experiments. Vydyanath et al. [24] deduced the vacancy-binding energy from electrical resistivity measurements for Mg–Zn, and Rao and Suryanarayana [25] used a Vickers hardness measurement method for Mg–Al. Their measured values are shown in Table 4 with our first-principles binding energies. There is a large discrepancy between the measured [25] and the calculated energy for Al–□ binding in Mg. Similar discrepancies for bindings in Al [5] were shown to be due to inaccuracies of non-equilibrium measurements. Hence, the discrepancy in Al–□ binding in Mg could be attributed to the method of Ref. [25] for determining equilibrium vacancy concentrations from hardness tests. Although our calculations for Zn–□ binding energy are in good agreement with Vydyanath et al. [24], this alone does not provide a critical test of the accuracy of our first-principles results. However, first-principles binding-energy calculations in Al [5] have been shown to be quantitatively accurate in comparison to equilibrium measurements. We thus call for future equilibrium measurements of solute–vacancy binding in Mg to test our predicted values.

Table 5 summarizes our calculated vacancy-binding energies for both NN and 2NN defect pairs for 34 elements in the present work. Further discussion of calculated binding energies can be found in the following sections.

4. Discussion

4.1. Physical contributions to solute–vacancy binding in Mg

4.1.1. Solute size

We next attempt to find the general trends and physical factors controlling solute–vacancy binding across all solutes that have been considered in the present work. Fig. 3 shows the calculated NN binding energies as a function of solute impurity volume, determined from Eq. (4).

Table 5
First-principles solute–vacancy binding energies in Mg. Given are binding energies for 64-atom cells, for both nearest-neighbor (NN) and second nearest-neighbor (2NN) solute–vacancy pairs. Positive energies indicate energetically favorable binding. Calculations are preformed using GGA as implemented in VASP.

Solute	Solute–vacancy binding energy (eV)	
	NN	2NN
Li	~0	~0
Na	0.07	−0.02
Al	0.03	0.01
Si	0.10	0.01
K	0.33	−0.06
Ca	0.06	0.08
Sc	−0.15	0.01
Ti	−0.21	0.04
V	−0.14	0.03
Cr	0.05	0.03
Mn	−0.06	0.03
Fe	−0.01	0.04
Co	0.16	0.06
Ni	0.16	0.05
Cu	0.08	0.03
Zn	0.05	0.01
Ga	0.05	~0
Ge	0.09	~0
As	0.14	0.02
Sr	0.21	−0.05
Y[a]	−0.07	~0
Zr	−0.24	0.03
Nb	−0.29	0.04
Mo	−0.22	0.05
Ag	0.05	0.02
Cd	0.05	0.01
In	0.06	−0.01
Sn	0.08	−0.01
Sb	0.13	−0.02
Pt	0.19	0.06
Au	0.11	0.03
Ba	0.52	−0.08
Pb	0.10	−0.02
Bi	0.14	−0.02

[a] 96-atom cell.

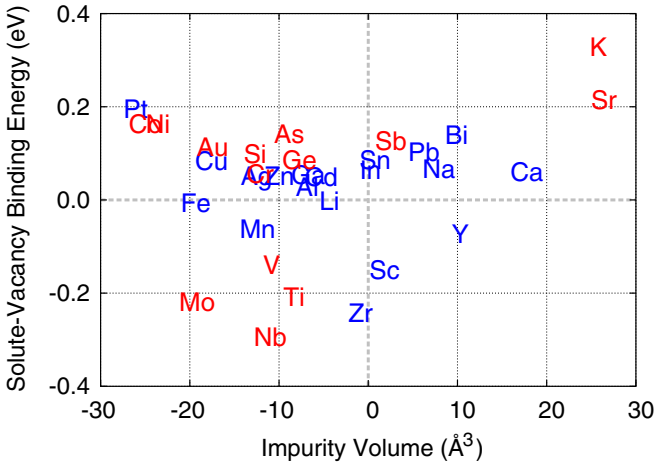

Fig. 3. First-principles calculated nearest-neighbor solute–vacancy binding energies as a function of solute impurity volume. The solute impurity volume is calculated from the volume change induced by adding a single impurity atom to pure Mg from Eq. (4). Elements in blue exhibit solubility in hcp Mg while those in red have essentially no solubility. (For interpretation of the references to colour in this figure legend, the reader is referred to the web version of this article.)

Except for the transition metals, there is a modest correlation between solute–vacancy binding and impurity volumes where larger solutes have larger binding energies with vacancies. A simple strain model could explain this correlation between the solute–vacancy binding and solute size. Placing a large impurity atom in Mg will induce a significant strain on the surrounding Mg atoms. In such instances, vacancies next to such large solute atoms will allow the solute atoms to relax towards the vacancy and to move further away from the neighboring Mg atoms. Thus, the vacancy at a NN position would partly relieve the strain of large solute atoms. Based on this simple model, one would expect stronger solute–vacancy binding energies as the size of solute increases.

At least for the very large impurities, we find this expected correlation between solute–vacancy binding and solute size. The largest impurity among the elements that have been considered in the present work is Ba and its vacancy binding energy is predicted as 0.52 eV, which is the largest among all the elements considered. K and Sr also have large impurity volumes and their vacancy-binding energies are 0.33 and 0.21 eV, respectively. These extremely large solute elements in impurity volume consequently yield extremely large strains in a Mg matrix, and hence very unfavorable dilute mixing energies. Therefore, these elements tend to exhibit little or essentially no solubility in Mg. We note that this simple strain model was also used to explain the trends of vacancy binding among various solutes in Al. Wolverton [5] investigated solute–vacancy binding energies in Al from first-principles density functional calculations,[2] and found a strong correlation (stronger than in the present case for Mg) between binding energy and solute size. Although this simple strain model completely ignores other factors that may affect the binding energy (e.g. chemical bonding and charge transfer), such strain-mediated behavior has been found in both Al and Mg alloys particularly for very large solutes, where we would expect strain arguments to dominate over chemical factors.

Another interesting observation can be found in Fig. 3 is that there is a trend between isoelectronic elements, i.e. Li/Na/K, Ca/Sr/Ba and Al/Ga/In, that larger atoms have stronger binding with vacancies. This trend also can be applied when comparing solutes in the same row of the periodic table, such as As/Ge/Ga/Zn and Ag/Cd/In/Sn.

In contrast to the strain argument, we find that even though dilute impurity volumes of Si, Ge and Sn are smaller than that of Mg, the binding energies of these elements with vacancies are predicted to be positive. Actually, many elements (e.g. Ga, Ge, As, Pt, Au and Ag) have positive solute–vacancy binding even though they have negative impurity volumes. On the contrary, Y has a fairly large volume as a dilute impurity in Mg, but is predicted to be repulsive with vacancies. Hence, the size of solute is clearly an important factor for binding with vacancies in Mg, but is not the only factor.

We also examine the effect of impurity volume on further neighbor solute–vacancy pairs. Fig. 4 shows the 2NN solute–vacancy binding energy with respect to the impurity volume. Overall, the magnitude of 2NN binding energies is much smaller than that of NN binding energies. There is a negative correlation between 2NN binding energies and impurity volumes, with larger solutes showing less favorable binding. A similar negative correlation was reported for the 2NN solute–vacancy binding in Al [5].

4.1.2. Binding with 3d metal solutes

As shown in Fig. 3, transition metals do not follow the correlation between binding energy and solute size, which

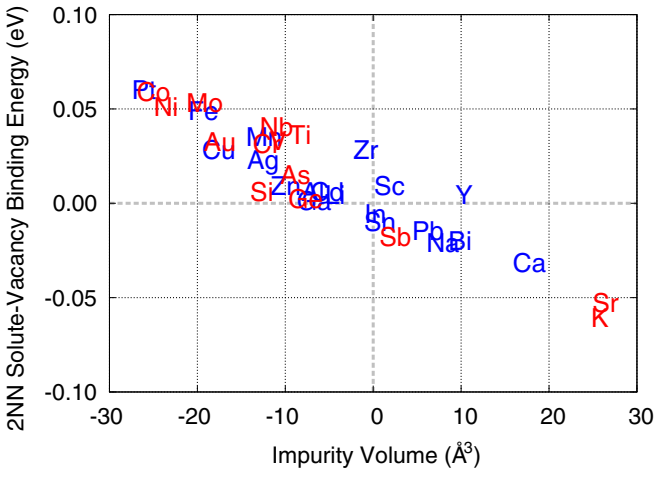

Fig. 4. First-principles calculated second nearest-neighbor solute–vacancy binding energies as a function of the solute impurity volume. The solute impurity volume is calculated from the volume change induced by adding a single impurity atom to pure Mg from Eq. (4).

[2] Ultrasoft-pseudopotentials (US-PP) as implemented in the VASP and used both the LDA and GGA for the exchange-correlation.

implies the importance of some physical effects other than strain for these elements. Fig. 5 shows the calculated NN and 2NN binding energies for solutes across the 3*d* metal series. Spin-polarized results for some solutes, e.g. Cr, Mn, Fe and V, are denoted as open symbols. Magnetic moments for these elements are summarized in Table 6. Spin-polarized calculations were also performed for Co and Ni, but their magnetic moments are found to be zero when embedded as impurities in a Mg matrix.

Fig. 5 shows a very interesting trend across the 3*d* transition metal series. Most early 3*d* metals, i.e. Ti, V, Cr, Mn and Fe, do not form favorable bonds with Mg. In binary Mg–X alloy systems with these elements, no ordered intermetallic compounds are experimentally observed. Also, these alloying elements in Mg tend to have positive mixing enthalpies in hcp Mg, often indicative of an energetic preference for phase separation. In Fig. 6, we show our calculated dilute mixing energies of the 3*d* solutes in Mg and compared with those from the COST 507 database [26], which are in quite good agreement. We also note that the solubility of these early 3*d* metals, Ti, V, Cr, Mn and Fe, in Mg is very limited; Mg–Ti and Mg–Cr even exhibit miscibility gaps in both the hcp and liquid phases.

Thus, one might expect from a simple bond-counting argument that these early 3*d* transition metals have favorable binding with vacancies since moving these solutes next

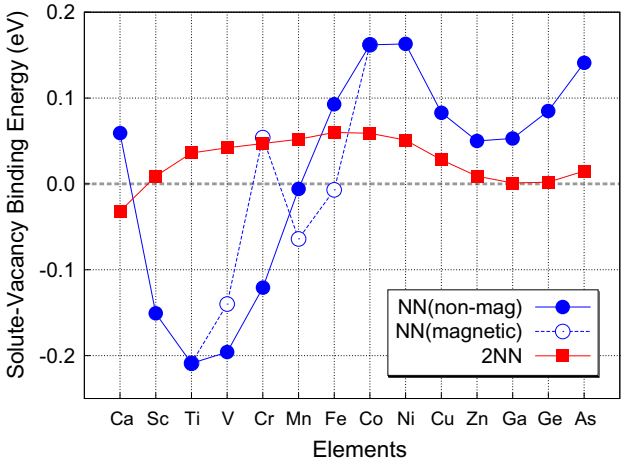

Fig. 5. First-principles calculated nearest-neighbor (NN) and second nearest-neighbor (2NN) solute–vacancy binding energies in hcp Mg across the 3*d* transition metal series. Results shown are for fully relaxed 64-atom supercells and spin-polarized results are denoted with open symbols.

Table 6
Predicted local magnetic moments of early 3*d* transition metals in $Mg_{63}X$ and $Mg_{62}X_1\square_1$ (for NN and 2NN) calculations.

Element	Magnetic moment (μ_B)		
	$Mg_{63}X$	NN	2NN
V	2.825	2.902	2.816
Cr	3.677	3.797	3.724
Mn	3.653	3.654	3.630
Fe	2.543	2.521	2.502

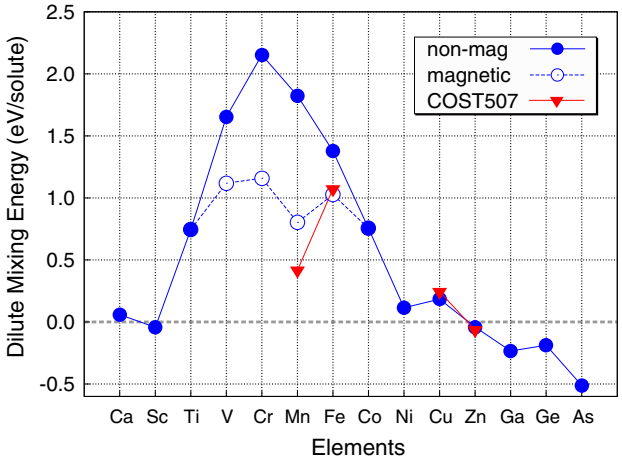

Fig. 6. First-principles calculated dilute mixing energies of the 3*d* series in Mg, compared with those from the COST 507 database [26]. Results shown are for fully relaxed 64-atom supercells and spin-polarized results are denoted with open symbols.

to a vacancy would eliminate one unfavorable Mg–X bond. However, our non-magnetic calculations indicate that only Fe and Co exhibit favorable binding with vacancies, while other early 3*d* transition metals, such as Ti, V and Cr, are strongly repelled from vacancies. In spin-polarized calculations, we obtained lower energy states of $Mg_{N-1}X_1$ and $Mg_{N-2}X_1\square_1$ for V, Cr, Mn and Fe. As a result, the dilute mixing enthalpies for V, Cr, Mn and Fe are predicted to be smaller (but still positive) than those from non-magnetic calculations. However, even the spin-polarized calculations do not support the simple Mg–X bond-counting model that would suggest a favorable binding of these early 3*d* solutes with vacancies. Only for Cr do we find a change in the sign for the vacancy-binding energy by considering the magnetism, and that of V is only slightly less repulsive with vacancies. For Mn and Fe, spin polarization made their binding with vacancies even more repulsive.

This complete failure of the bond-counting argument in Mg is interesting, because it has been used to explain solute–vacancy binding of early 3*d* transition metals in Al: Hoshino et al. [27] and Wolverton [5] have previously studied the interaction between 3*d* solutes and vacancies in Al through first-principles density functional calculations. Wolverton [5] used ultrasoft-pseudopotentials with a fully relaxed supercell with respect to all degrees of freedom, whereas Hoshino et al. [27] have used the full-potential Korringa–Kohn–Rostoker (KKR) Green's function total-energy method, but constrained all atoms to be at the perfect face-centered cubic (fcc) Al lattice sites. Despite the different relaxation schemes, both sets of authors obtained the same trend of negative binding between 3*d* solutes and vacancies, indicating 3*d* solutes are repelled from vacancies. Hoshino et al. [27] suggested that the strong repulsion can be understood by essentially the same simple bond-counting model described above. All the early 3*d* transition metals are experimentally known to form stable intermetallic compounds

with Al, indicating strong Al–X bonds due to *sp–d* hybridization between Al and X. Thus, placing a vacancy next to 3*d* solutes is essentially unfavorable, since it requires breaking one strong Al–X bond. Consequently, most early 3*d* solutes, such as Ti and V, are strongly repelled from vacancies. Mg provides precisely the opposite case from Al, i.e. unfavorable Mg–X bonds—manifested by no intermetallic compounds and limited solubility in Mg–X phase diagrams—which would then suggest attractive solute–vacancy binding. However, only Co (and maybe Cr) has positive binding as postulated, while all the other early 3*d* transition metals are strongly repelled from vacancies in Mg. Thus, the binding of 3*d* solutes with vacancies in Mg cannot be explained by a simple bond-counting model, even though this simple argument appears to explain the repulsion of 3*d* solutes and vacancies binding in Al.

4.1.3. Effects of solute atoms on the lattice parameters of Mg

In the previous sections, we found two examples in which interaction between solute atoms and vacancies in Mg is far more complex than that in Al. Both fcc Al and hcp Mg are closed-packed structures and commonly have 12 NN bonds, however, fcc Al has 12 equivalent NN bonds, while hcp Mg has two different types of inequivalent NN bonds: the first six bonds are the ones with Mg atoms on the basal plane and the second six bonds are the ones with Mg atoms out of the basal plane. Due to the slight distortion of the c/a ratio of Mg from ideal hcp, the lengths of two different NN bonds in Mg are not identical. Hence, we wish to investigate the effect of single solute atom on the lattice parameters of hcp Mg.

Fig. 7 shows the correlation between a and c lattice parameters for impurities in Mg for all elements considered in the present work. The lattice parameters of the defect-free supercell and the one with a vacancy at the origin are represented as Mg and Va in the plot, respectively. The diagonal line in Fig. 7 represents the c/a ratio of defect-free hcp Mg and any deviation from this line is an indication of anisotropic relaxation upon the addition of a single solute atom. We note that this type of anisotropic relaxation is not allowed by symmetry in fcc elements, such as Al. Fig. 7 shows that many elements cause anisotropic relaxation of hcp Mg and a resulting change in c/a ratio. The large solutes, such as Ca, K, Sr and Ba, increase both lattice parameters a and c significantly, and interestingly Ba increases a far more than c, and thus gives an anisotropic relaxation far from the diagonal line in Fig. 7. On the other hand, Y and Bi have similar impurity volumes in Mg as shown in Fig. 3, and they both give the same peculiar elongation of Mg almost purely along the c-axis. (Y significantly expands c, but contracts a.) Additions of As, Ge and Si are also quite interesting. Although their atomic radii are similar (As 1.25, Ge 1.23, Si 1.17 Å), only Si decreases the lattice parameters of both a and c for Mg, while As and Ge only decrease a, indicating only the Mg atoms on the basal plane relax towards As and Ge. Hence, we see that the atomic relaxation to relieve the strain induced by putting a solute atom in a Mg matrix is quite complicated due to the two degrees of freedom along the a and c axes of hcp. The presence of a vacancy next to the solute atoms makes the relaxation even more complex, and thus it is perhaps not surprising that simple strain and bond-counting models do not fully explain solute–vacancy binding in Mg.

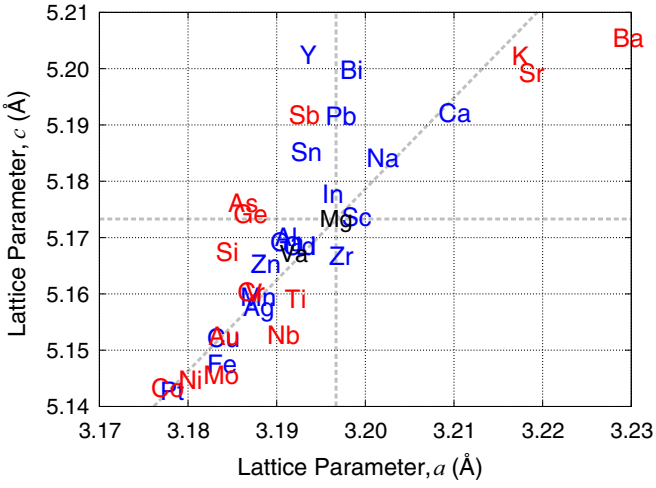

Fig. 7. First-principles calculated effect of a single solute atom on the a and c lattice parameters of 64-atom hcp Mg supercells. Mg and Va in the plot represent the lattice parameters of a defect-free supercell and one with a vacancy at the origin, respectively. The diagonal line represents the c/a ratio of hcp Mg and deviation from this line indicates an anisotropic relaxation.

4.2. Solute–vacancy binding of microalloying additions to Mg alloys: Na, In, Zn, Ag and Ca

Very recently, Mendis et al. [1] observed that small additions of Na and In + Li in Mg–Sn alloys promoted age hardenability by refining the precipitate distribution. Mendis et al. [2] also found that microalloying of Zn and Zn + Na in the same alloy resulted in a substantial increase in hardening; however, these additions increased the density of precipitates only modestly. They concluded that enhanced hardening response is mainly attributed to the change in particle morphology and thus the increased probability of these precipitates interacting with dislocations gliding on basal planes. Mendis et al. [4] reported in a more recent paper that microalloying additions of Ag and Ag + Ca significantly improve the age-hardening response in Mg–Zn alloys. They concluded that the enhanced age-hardening response in Mg–Zn alloys is due to the refinement of the precipitates although the mechanism of the precipitate refinement has not yet been verified.

Although the mechanism of the improved age-hardening response in Mg alloys due to microalloying additions is not fully understood, we suggest that the binding energetics between vacancies and microalloying solutes in Mg would provide useful insight. Mendis et al. [1] elucidated that Na microalloying additions to Mg–Sn alloys is analogous to the effect of Sn, In or Cd additions in Al–Cu alloys. These

microalloying additions increase the hardening response of artificially aged Al–Cu, but also decrease the natural aging response [28,29]. This decreased natural aging has been attributed to the binding between vacancies and solute elements. Kimura and Hasiguti [30] suggested that a stronger Sn–vacancy binding compared to Cu–vacancy binding starves vacancies for Cu and diminishes diffusion, and thus suppresses the formation of Cu clusters or Guinier–Preston zones, responsible for the natural aging response in Al–Cu alloys. Ringer et al. [31] also speculated in recent work that the competition for vacancies between solutes in an Al–1.7Cu–0.3Mg–0.1Ge alloy during the early stages of aging is a key consideration in determining which precipitate nucleation processes occur.

We then wish to examine the solute–vacancy bindings for the observed microalloying of Na, In and Zn in Mg–Sn and Ag and Ca in Mg–Zn. Interestingly, our first-principles NN vacancy-binding energies for the elements that have been experimentally shown to improve mechanical properties of Mg alloys, i.e. Na, In, Zn, Ag and Ca, in Table 5 all have favorable binding with vacancies in Mg: 0.07, 0.06, 0.05, 0.05 and 0.06 eV, respectively. However, in all cases, the vacancy binding of microalloying solutes is nearly the same as the major alloying element in the observed Mg–Sn and Mg–Zn systems: vacancy-binding energies of Na, In, Zn in Mg are slightly smaller than that of Sn (0.08 eV), and those of Ag and Ca are also the same as that of Zn (0.05 eV).

It should be emphasized here that we are not suggesting a mechanism between the solute–vacancy binding energetics in Mg and the enhanced mechanical properties of Mg alloys, but simply reporting an observed correlation. Our calculations predict that Ga and Cd have binding energies close to 0.05 eV, suggesting that a study of these microalloying additions to Mg alloys could be of interest. In addition, Cu and Sn are predicted to have larger vacancy-binding energies of 0.08 eV, and Pb, Bi and Pt have ever larger vacancy binding energies of 0.10, 0.14 and 0.19 eV, respectively. To our knowledge, microalloying of these elements in Mg alloys has not been attempted, but such experiments would provide a very interesting test of this correlation.

5. Summary

In summary, we have computed a large database of solute–vacancy binding energies in Mg from first-principles calculations. We could not directly compare our first-principles binding energies with experiments due to the scarcity of accurate measurements for vacancy binding energy in Mg, but our calculated bindings serve as predictions to be tested by future experiments. Nevertheless, our monovacancy formation energy as well as dilute mixing energies and structural relaxation of various solutes in hcp Mg, which are by-products of first-principles solute–vacancy binding energy calculations, show good agreement with experimental data, where available.

We analyze the trends of solute–vacancy binding energies across all solutes that have been considered to correlate them with simple physical factors. We find a moderate correlation between solute–vacancy binding energy and solute impurity volume where larger solutes more favorably bond to vacancies. A simple strain model can account for this correlation. For early 3*d* transition metal solutes, simple strain or bond-counting models alone cannot explain the trend of unfavorable binding between solutes and vacancies in Mg.

We have also investigated the changes in lattice parameters induced by alloying additions of solutes in hcp Mg. We find that the relaxation of surrounding Mg atoms is rather complicated due to the anisotropy of the hcp structure which has two degrees of freedom, *a* and *c*. Several solutes exhibit a strong anisotropic relaxation of *a* and *c* in hcp Mg, and our first-principles calculations successfully reproduce these complex relation behaviors.

Our calculations predict favorable binding with vacancy in Mg for the microalloying elements that are experimentally known to increase the age-hardening response in Mg alloys, i.e. Na, In and Zn in Mg–Sn and Ag and Ca in Mg–Zn, respectively. However, we emphasize that we are not suggesting a mechanism for the increased age-hardening response in Mg-alloys due to microalloying, but rather a simple correlation with positive binding energies at this point. In addition, our calculations predict several elements will have even larger binding energies (Cu, Sn, Pb, Bi and Pt) and these predictions are awaiting experimental testing.

Acknowledgments

This work was funded by the US Automotive Materials Partnership Project on ICME for Magnesium. This material is based upon work supported by the Department of Energy National Energy Technology Laboratory under Award Nos. DE-FC05-95OR22363, DE-FC05-02OR22910 and DE-FC26-02OR22910.

References

[1] Mendis CL, Bettles CJ, Gibson MA, Gorsse S, Hutchinson CR. Philos Mag Lett 2006;86:443.
[2] Mendis CL, Bettles CJ, Gibson MA, Hutchinson CR. Mater Sci Eng A 2006;435:163.
[3] Mendis CL, Muddle BC, Nie JF. Philos Mag Lett 2006;86:755.
[4] Mendis CL, Oh-ishi K, Hono K. Scripta Mater 2007;57:485.
[5] Wolverton C. Acta Mater 2007;55:5867.
[6] Kresse G, Furthmüller. J Comput Mater Sci 1996;6:15.
[7] Kresse G, Furthmüller. J Phys Rev B 1996;54:11169.
[8] Kresse G, Joubert D. Phys Rev B 1999;59:1758.
[9] Perdew JP, Wang Y. Phys Rev B 1992;45:13244.
[10] Perdew JP, Chevary JA, Vosko SH, Jackson KA, Pederson MR, Singh DJ, et al. Phys Rev B 1992;46:6671.
[11] Vosko SH, Wilk L, Nusair M. Can J Phys 1980;58:1200.
[12] Balluffi RW, Ho PS. In: Aaronson HI, editor. Diffusion. Metals Park, OH: American Society for Metals; 1973. p. 83.
[13] Beevers CJ. Acta Metall 1963;11:1029.
[14] Mairy C, Hillaire J, Schumach D. Acta Metall 1967;15:1258.
[15] Janot C, Mallejac D, George B. Phys Rev B 1970;2:3088.

[16] Tzanetakis P, Hillairet J, Revel G. Phys Stat Solidi B 1976;75:433.
[17] Vehanen A, Rytsölä K. In: Brandt W, editor. Proceedings of the international school of physics. Utrecht: North-Holland; 1981.
[18] Chetty N, Weinert M, Rahman TS, Davenport JW. Phys Rev B 1995;52:6313.
[19] Krimmel H, Fahnle M. Phys Rev B 2000;62:5489.
[20] Ceperley DM, Alder BJ. Phys Rev Lett 1980;45:566.
[21] Perdew JP, Zunger A. Phys Rev B 1981;23:5048.
[22] Carling K, Wahnstrom G, Mattsson TR, Mattsson AE, Sandberg N, Grimvall G. Phys Rev Lett 2000;85:3862.
[23] Nayeb-Hashemi AA, Clark JB. Phase diagrams of binary magnesium alloys. Metals Park, OH: ASM International; 1988.
[24] Vydyanath HR, Sastry DH, Vasu KI. Phys Status Solidi 1968;29:K137.
[25] Rao AR, Suryanarayana C. Phys Status Solidi A 1978;45:K131.
[26] Ansara I, Dinsdale AT, Rand MH. Thermochemical database for light metal alloys: European Cooperation in the Field of Scientific and Technical Research; 1998.
[27] Hoshino T, Zeller R, Dederichs PH. Phys Rev B 1996;53:8971.
[28] Ringer SP, Hono K, Sakurai T. Metall Mater Trans A 1995;26:2207.
[29] Bourgeois L, Nie JF, Muddle BC. Philos Mag 2005;85:3487.
[30] Kimura H, Hasiguti RR. Acta Metall 1961;9:1076.
[31] Ringer SP, Prasad KS, Quan GC. Acta Mater 2008;59:1933.
[32] Monkhorst HJ, Pack JD. Phys Rev B 1976;13:5188.